Journal of Harbin Engineering University Vol 45 No. 7
ISSN: 1006-7043 July 2024

Numerical Investigation of Heat Transferred Enhancement in Nano-fluid Flow through Elastic Conduit Channel

[1]Oyetunde Adeoye ADEAGA 0000-0003-0690-5874, **[2]Rotimi Adedayo IBIKUNLE** 0000-0002-8622-8422 **[3]Oluwaseyi Omotayo ALABI** 0009-0005-0027-5930, **[4]Timothy Adewale ADEYI** 0000-0002-1042-227X, **[4]Sakiru Kayode EKUN** 0009-0003-8477-7465

[1]Department of Mechanical and Mechatronics Engineering,
First Technical University, Ibadan, Nigeria
[2]Department of Department of Mechanical Engineering,
Affordable and Clean Energy Research Group, SDG7,
Landmark University, Omu-Aran, Kwara State, Nigeria.
[3]Department of Mechanical Engineering University of Ibadan, Nigeria.
[4]Department Mechanical Engineering Lead City University, Ibadan, Nigeria

Abstract

Heat transferred during fluid flow in conduit is a concern of design engineers. In this article, numerical models had been explored to investigate heat transferred within Nano-fluid in state of aqueous suspensions of 0.2% volume of Graphene-Oxide and water (GO/water) at constant heat flux. Numerical model captured geometrical and physical properties of uniform elastic pipe channel and fluid flow phenomena within the control volume. Nano-fluid was suspended with a view to enhancing the heat transfer rate and thermal performance. Constitutive equations of fluid flow with Navier-Stokes equations and energy equation for heat transfer were explored and solutions obtained numerically. Boundary temperatures were captured such that inlet temperature of 288 K and thermal boundary conditions were applied during investigation. Fill- ratio of 50%, 60%, 70%, 80%, 90%, 100% were considered at interval of 6 hrs. for 24 hrs. for heat loads of between 5W and 30W at intervals. With 0.20vol. % GO/water, Nano-fluids, maximum coefficient of heat transferred occurs at the highest heat load at 30W for 50% fill ratio and less heat-transfer coefficient at heating power of 10 W. This article therefore displays potential of numerical investigation in the analysis of thermal distribution within regular conduit.

List of Keywords: Heat transfer coefficient, Heat load, Conduit flow, Numerical method, Nusselt number

1. Introduction

Ubiquitous nature of heat transferred as a critical aspect of industrial processes cannot be overstated. Its significance is multifaceted, ranging from system design optimization to facilitating the smooth operation of machinery and equipment. In essence, heat transfer acts as a crucial underpinning for the effective functioning of industrial systems [1]. The inclusion of nanoparticles in a fluid can alter its transport and thermal properties, thereby modifying its fundamental characteristics, [2] [3]. For instance, nanoparticles added to a fluid can increase its thermal conductivity in an unconventional way by facilitating heat transfer [4]. Moreover, nanoparticles can augment the fluid's potential to exchange energy, a pivotal characteristic in a multitude of industrial applications. Research by [5] showed that Nano-fluids outperformed both liquid nitrogen and water coolants in terms of microchannel heat exchanger cooling rates. Meanwhile, [6] delved into convective heat transferred performance in organic solvents during laminar and turbulent flows in tubes, finding that Nano-fluids exhibit greater heat transfer performance compared to conventional fluids for similar Reynolds numbers.

Choi and Eastman [4][7] introduced the concept of nanoparticle dispersions in base fluids. A variety of materials have been utilized as nanoparticles, including some metals (Al, Cu), carbides (SiC), and Oxides (Al_2O_3), while water and methanol are often base fluids. Studies have demonstrated altering concentration, size, shape, material of nanoparticles can impact thermal conductivity in Nano-fluids [7].Thermal Conductivity in Nano-fluids is heavily influenced by nature of the nanoparticles, with shape and material composition playing a

crucial role [8] [9]. The improved heat transfer properties of Nano-fluids can translate to energy savings [7] [10], increased equipment longevity, and enhanced productivity in various industrial applications [11]. Micro channels, extended surfaces, and other methods can further enhance heat transfer efficiency, and there's a wealth of research on the physical characteristics of Nano-fluids and their effects on flow within boundary layer [12]. It is to be noted that simulation studies are performed to quantify certain uncertainties from solutions that are usually iterative in nature with iteration value carefully chosen [26] [27].

Heat transfer in pipe channels is a crucial aspect of numerous engineering applications, such as thermal systems, energy conversion systems, and fluid transport systems [13][14]. The qualities of a substance related to its thermal and physical behavior are referred to as its thermo-physical properties [15][16][17]. The optimization of the performance and efficiency of these systems hinges on understanding the factors that impact heat transfer characteristics [18][16]. While rigid pipe channels have been extensively studied, the evaluation of heat transfer in elastic pipe channels under varying temperature conditions has been relatively unexplored. A key feature of elastic pipe channels is their ability to undergo small deformations in response to temperature gradients [19] [20]. These deformations introduce complexity to the heat transfer process, impacting temperature distribution, flow patterns, and heat transfer rates [21] [22].

Researchers have utilized experimental, computational, and numerical approaches to study heat transfer in pipe flow, focusing on operational parameters such as heat flux, tilt angle, working fluid fill, and nanoparticle concentration. Sarafraz and Hormozi (2014), examined effects of these variables on efficiency and performance of thermosyphon pipe [4]. As reported, increasing the fill ratio resulted in an 18% boost in entrainment. Relatedly, thermal performances in pulsating closed loop was evaluated with ethanol and water at fill ratios, 28%, 41.3%, 63%, 82.5% and 100% [23]. For water, at low input heat, low filling ratio led to lower thermal resistance and optimal heat transferred. For ethanol, low heat input, higher filling ratio resulted in better performance beyond 50%.

In [24], a computational study employing the finite volume method was performed to analyze free convective heat-transferred in concentric square annuli. Influences of various geometrical parameters, such as aspect ratio, Rayleigh number, and Prandtl number, on heat transferred were investigated in this article. The results showed that increasing the Rayleigh number enhances heat transferred, while increasing the aspect ratio reduces it. Additionally, higher Prandtl numbers correspond to slower heat transfer rates, significantly impacting heat transfer performance. The study's main takeaway is that various geometric factors have a significant impact on heat transfer through natural convection in a concentric square annulus. In a separate study numerical method was explored to investigate heat transferred due to natural convection in a porous enclosure filled with Ag-M_gO hybrid/water Nano-fluid. Local thermal non-equilibrium model was explored to account for temperature differences inbetween solid and fluid phases. Several characteristics that impact heat transfer and fluid flow were investigated, such as nanoparticle volume percentage, Rayleigh number, and Darcy number. The findings revealed that heat transfer is enhanced in the hybrid Nano-fluid when compared to pure water. Furthermore, an increase in the Rayleigh and nanoparticle volume fractions results in enhanced heat transfer. [25]

This study investigated heat transfer enhancement of graphene-oxide (GO) Nan0-fluid in an elastic pipe flow with various filled ratios (FR) of 50% to100% and at different heat load of 5W to 30W, a variety of numerical and computational solvers/tools to gain a deeper understanding of convective heat transfer flow. These tools include: Computational Fluid Dynamics Solvers: Ansys Fluent, COMSOL Multi-Physics, etc. CAD tools: SolidWorks, Autodesk Inventor, AutoCAD, Corel Draw, etc.

Simulations were conducted for 0.2% volume of Graphene-Oxide and water (GO/Water) Nano-fluid with the help of Computational Fluid Dynamics (CFD) module. Temperature profiles, heat transfer coefficient and Nusselt number (Nu) were presented. Simulations involve solving the heat transfer and fluid flow equations in an elastic pipe

channel at various heat load and at filling ratio of 50%. The findings will reveal crucial insights into how GO/water Nano-fluid perform when transferring heat in elastic pipe channel at different temperatures. The research will help develop fluid systems that are reliable efficient and capable of functioning in high-temperature environment.

2. Methodology

The model is governed by continuity equation and the Navier-Stokes equations, with undelisted assumptions: (i) steady-state, laminar natural convection of nano-fluid; (ii) inlet temperature of 288 K; (iii) gravity neglected; (iv) continuous heat flux as the thermal boundary condition; and (v) no-slip condition at walls.

2.1 Formulation of Governing Equations

2.1.1 Continuity Equation

(1) is continuity equation in form of numerical model

$$\frac{\partial U_r}{\partial r} + \frac{1}{r}\frac{\partial U_\emptyset}{\partial \emptyset} + \frac{\partial U_x}{\partial x} = 0 \quad (1)$$

U x is non-zero velocity component, *r* is non-dimensional radial coordinate, ϕ is non-dimensional azimuthal coordinate, and *x* is non-dimensional axial coordinate, thus

U r = *U* ϕ= 0.

U_x is non zero velocity component, thus

$$U_r = U_\emptyset = 0 \quad (2)$$

(1) becomes;

$$\frac{\partial U_x}{\partial x} = 0 \quad (3)$$

Equation 3 confirmed U_x not dependent on radial component of pipe implied thinned wall pipe and $U_x = U_x(r)$ is same for all x.

$$U_x = U_x(r) \quad (4)$$

2.1.2 Momentum equation

Radial direction:

$$\rho\left(\frac{\partial U_r}{\partial t} + U_r\frac{\partial U_r}{\partial r} + \frac{U_\emptyset}{r}\frac{\partial U_r}{\partial \emptyset} + U_x\frac{\partial U_r}{\partial x} + \frac{{U_\emptyset}^2}{r}\right) = \rho g_r - \frac{\partial P}{\partial r} + \mu\left[\frac{\partial^2 U_r}{\partial r^2} + \frac{1}{r^2}\frac{\partial^2 U_r}{\partial \emptyset^2} + \frac{\partial^2 U_r}{\partial x^2} + \frac{1}{r}\frac{\partial U_r}{\partial r} - \frac{2}{r^2}\frac{\partial U_\emptyset}{\partial \emptyset} - \frac{U_r}{r^2}\right] \quad (5)$$

Azimuthal direction

$$\rho\left(\frac{\partial U_\emptyset}{\partial t} + U_r\frac{\partial U_\emptyset}{\partial r} + \frac{U_\emptyset}{r}\frac{\partial U_\emptyset}{\partial \emptyset} + U_x\frac{\partial U_\emptyset}{\partial x} + \frac{{U_\emptyset}^2}{r}\right) = \rho g_\emptyset - \frac{\partial P}{\partial \emptyset} + \mu\left[\frac{\partial^2 U_\emptyset}{\partial r^2} + \frac{1}{r^2}\frac{\partial^2 U_\emptyset}{\partial \emptyset^2} + \frac{\partial^2 U_\emptyset}{\partial x^2} + \frac{1}{r}\frac{\partial U_\emptyset}{\partial r} + \frac{2}{r^2}\frac{\partial U_r}{\partial \emptyset} - \frac{U_\emptyset}{r^2}\right] \quad (6)$$

Axial direction

$$\rho\left(\frac{\partial U_x}{\partial t} + U_r\frac{\partial U_x}{\partial r} + \frac{U_\emptyset}{r}\frac{\partial U_x}{\partial \emptyset} + U_x\frac{\partial U_x}{\partial x}\right) = \rho g_x - \frac{\partial P}{\partial x} + \mu\left[\frac{\partial^2 U_x}{\partial r^2} + \frac{1}{r^2}\frac{\partial^2 U_x}{\partial \emptyset^2} + \frac{\partial^2 U_x}{\partial x^2} + \frac{1}{r}\frac{\partial U_x}{\partial r}\right] \quad (7)$$

Substitute equation 2 and 3 into equation 5 and 6,

$$\frac{\partial P}{\partial r} = 0 \quad (8)$$

$$\frac{\partial P}{\partial \emptyset} = 0 \quad (9)$$

From (8) and (9),

$$\frac{\partial P}{\partial r} = \frac{\partial P}{\partial \emptyset} = 0 \quad (10)$$

(10) is pressure dependence on axial-direction only. Substitution of (2) and (3) into (10) and imposing steady state condition yields;

$$\frac{\partial U_x}{\partial t} = 0 \quad (11)$$

$$0 = \rho g_x - \frac{\partial P}{\partial x} + \mu\left[\frac{\partial^2 U_x}{\partial r^2} + \frac{1}{r^2}\frac{\partial^2 U_x}{\partial \emptyset^2} + \frac{\partial^2 U_x}{\partial x^2} + \frac{1}{r}\frac{\partial U_x}{\partial r}\right] \quad (12)$$

Rearranging

$$\frac{\partial P}{\partial x} = \rho g_x + \mu\left[\frac{\partial^2 U_x}{\partial r^2} + \frac{1}{r^2}\frac{\partial^2 U_x}{\partial \emptyset^2} + \frac{\partial^2 U_x}{\partial x^2} + \frac{1}{r}\frac{\partial U_x}{\partial r}\right] \quad (13)$$

By applying eqn. (2) and neglecting gravitational effect

$$\frac{\partial P}{\partial x} = \mu\left[\frac{\partial^2 U_x}{\partial x^2}\right] \quad (14)$$

(3) and (14) are momentum transport equations for the model.

Energy Equation

Steady flow energy transmission equation is;

$$k\frac{\partial^2 T}{\partial r^2}+\frac{k}{r^2}\frac{\partial^2 T}{\partial \emptyset^2}+\frac{\partial^2 T}{\partial x^2}+\frac{k}{r}\frac{\partial T}{\partial r}+\emptyset_{(i)}=\rho C_p\left[U_r\frac{\partial T}{\partial r}+U_\emptyset\frac{\partial T}{\partial \emptyset}+U_x\frac{\partial T}{\partial x}\right]$$

(15)

Substituting the viscous dissipation, term $\emptyset_{(i)}$ into (2) gives:

$$k\frac{\partial^2 T}{\partial r^2}+\frac{k}{r^2}\frac{\partial^2 T}{\partial \emptyset^2}+\frac{\partial^2 T}{\partial x^2}+\frac{k}{r}\frac{\partial T}{\partial r}=\rho C_p\left[U_r\frac{\partial T}{\partial r}+U_\emptyset\frac{\partial T}{\partial \emptyset}+U_x\frac{\partial T}{\partial x}\right] \quad (16)$$

U_x is non-zero velocity component. Dividing (2) throughout by 'k' will lead to:

$$\frac{\partial^2 T}{\partial x^2}+\frac{1}{r}\frac{\partial T}{\partial r}=\frac{\rho C_p}{k}\left[U_x\frac{\partial T}{\partial x}\right]$$

(17)

with, $\alpha=\frac{k}{\rho C_p}$

(18)

Equation (12) reduces to

$$\frac{\partial^2 T}{\partial x^2}=\frac{U_x}{\alpha}\frac{\partial T}{\partial x}$$

(19)

(19) is energy transport equation for fluid flow within pipe.

2.2 Computational modeling and simulation

This involves examining parameters such as temperature profiles, Nusselt number, and convective heat transfer coefficients. COMSOL Multi-Physics 6.0 was employed to create a computational model of the elastic pipe shown in Figure 1 (a), with Figure 1 (b) representing the generated mesh domain.

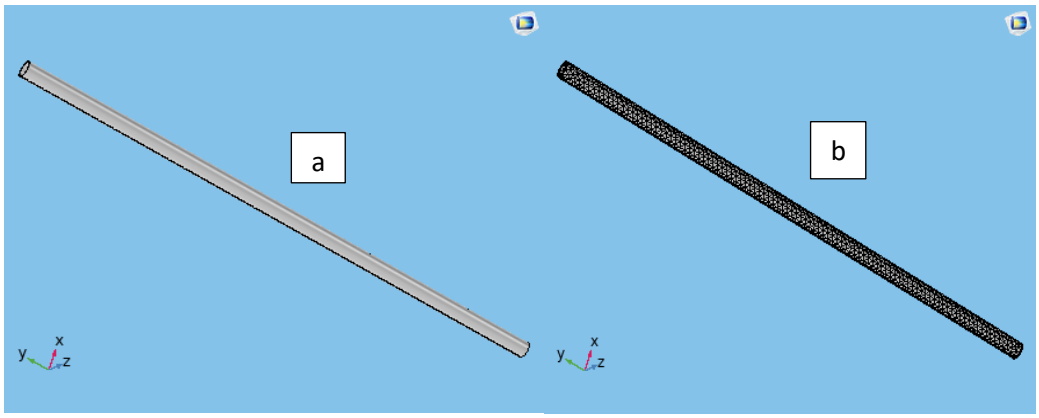

Figure 1: (a) Elastic pipe (b): Mesh generated

4.0 Results and discussion

4.1 Thermal Behaviors

The heat transport was assessed using the equation below:

$$h=\frac{q}{Ae(T_w-T_b)}$$

(20)

Where T_w is wall temperature

T_b is bulk temperature of the fluids

$$Nu=\frac{(0.125f)(re-1000)Pr}{1.07+12.7\sqrt{0.125f(Pr^{\frac{2}{3}}-1)}}$$

(21)

where

$$f=(1.82\log_{10}(Re)-1.64)^{-2}$$

(22)

Nusselt number was derived from the heat transfer coefficient in fully-developed fluid flow region in term of hydrodynamics and heat transfer.

Mixture of graphene-oxide and water (GO/Water) exhibit distinctive thermal behaviors, referring to their response to temperature variations and ability to transfer heat as shown in figs. 4,5,6, and 7 at different filling ratio at different time interval. Figure 3 shows the temperature distribution at time T = 60 min. for initial temperature of 288k for different filling ratio. The temperature is gradually developed and constant all the filling ratio. The system's performance and heat transfer characteristics can be impacted by this Nano-fluid (GO/Water). Figs. 5, 7, and 8 illustrate the rise in temperature from the pipe flow inlet to the outlet for the working fluid for different filling ratio. The temperature increase is caused by the expansion of the fluid as it flows toward the outlet, with the pulsing section of the pipe transferring energy to other fluids, which can cause heat loss and sweating. Also, there is increase in

temperature as along stream flow of fluid as fill ratio increases with time. Across range of fill ratio, heat transferred coefficient within pipe, increase with concentration of GO nanoparticles in base fluid, illustrating boosting effect of Nano-particles on heat transferred.

Effects of heating power and fill ratio on the heat transfer coefficient of GO/water Nano-fluids are illustrated in Fig. 8 which further shows that heat transferred coefficient within pipe rises with increasing input heat power, when the fill ratio is 50%. Increase in heat transferred coefficient at higher loads of heat were due to acceleration of vaporization and bubble formation in the working fluid. Moreover, higher heat load lead to higher nucleation sites and high formation rate bubbles which eventually facilitates faster vaporization of the GO/water Nano-fluids. For 50% fill ratio, GO/water Nano-fluids with 0.20vol.% concentration exhibited maximum heat transfer coefficient at heat load of 30 W, whereas lower heat loads result in lower heat transfer coefficients.

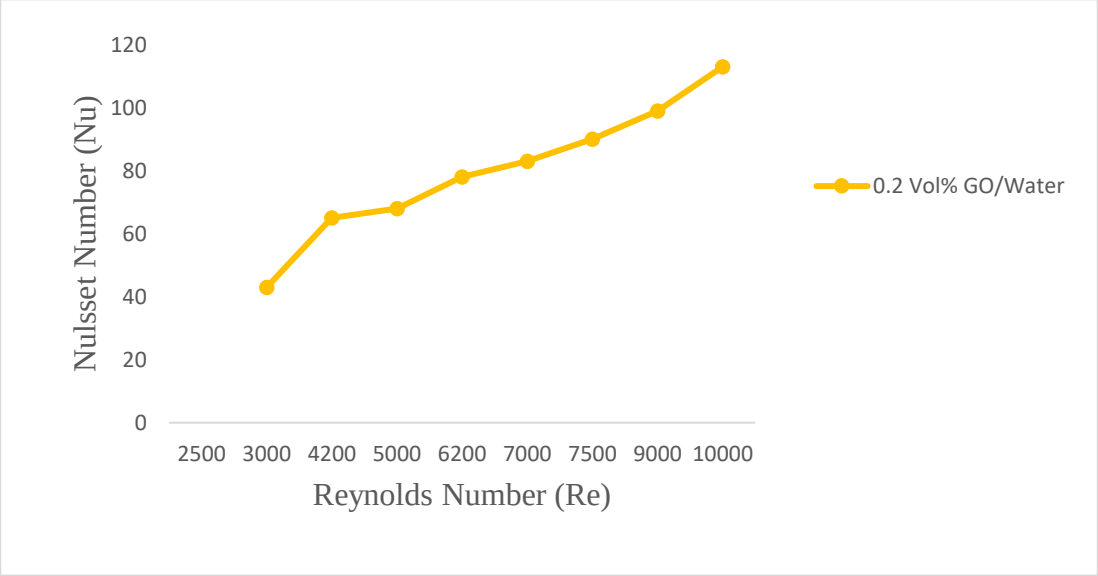

Fig. 2: Nusselt versus Reynolds number for Graphene Oxide Nano-fluid

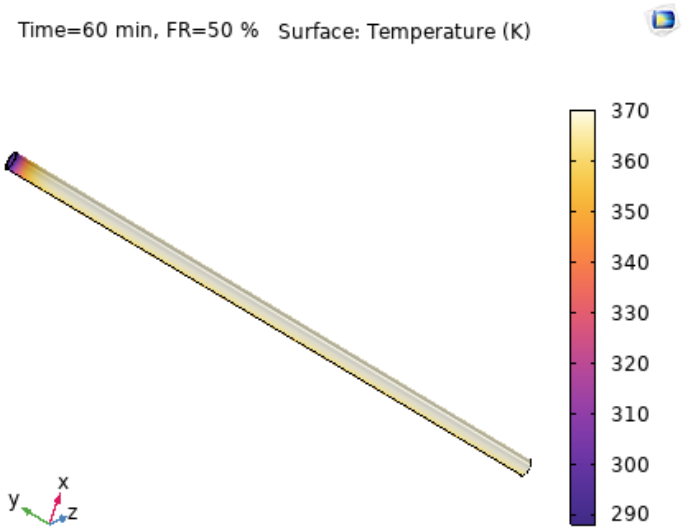

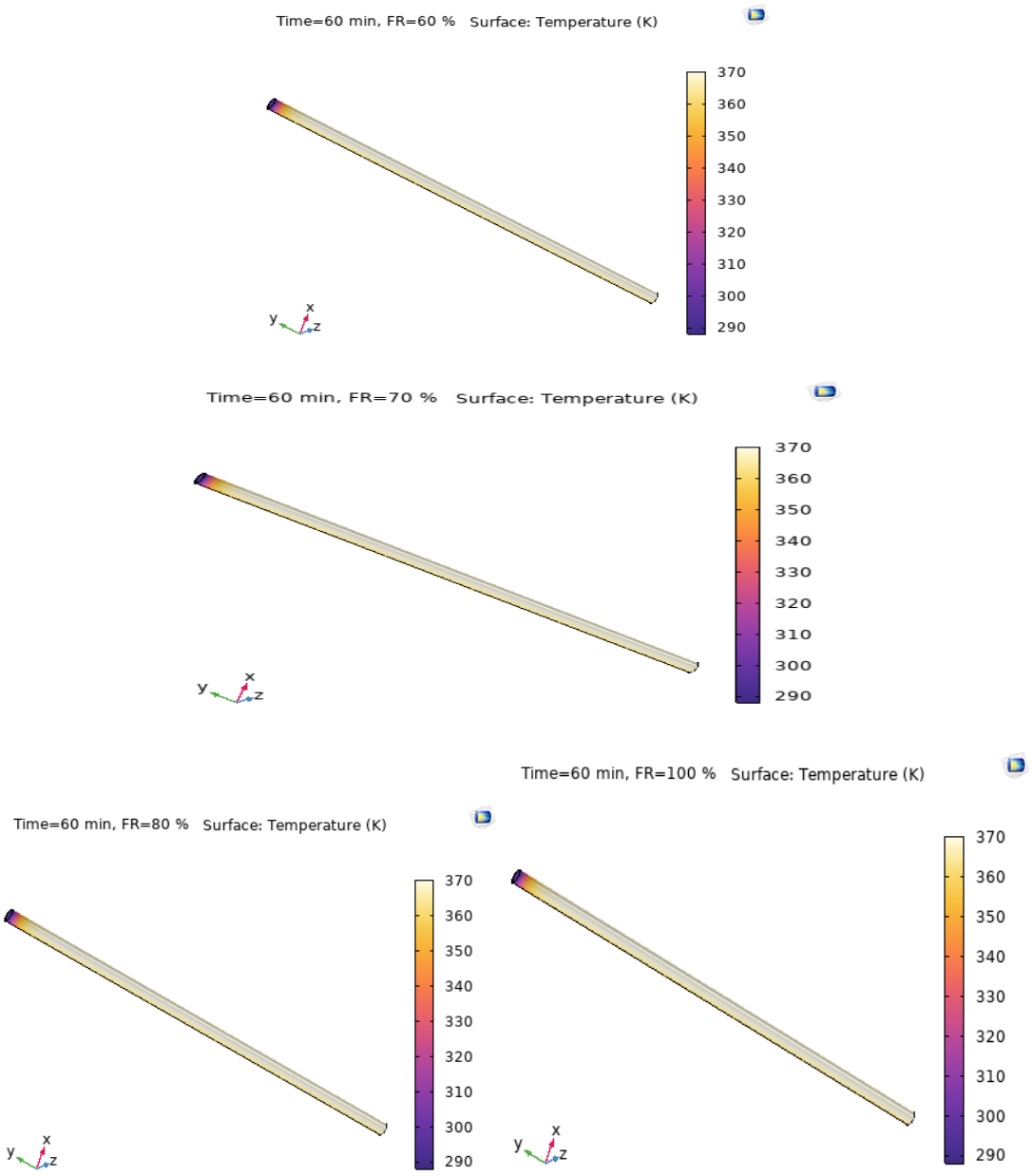

Figs. 3: Thermal distribution at different fill ratios, when T = 60min

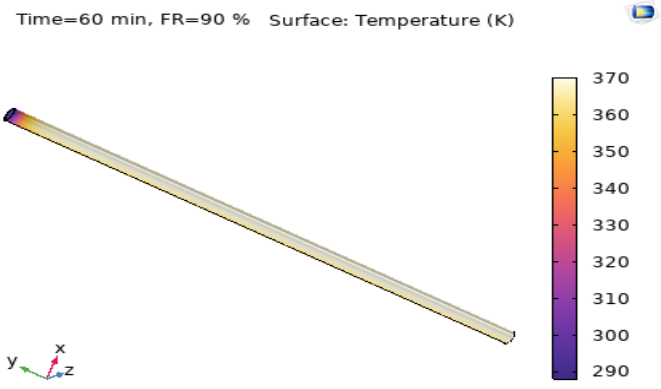

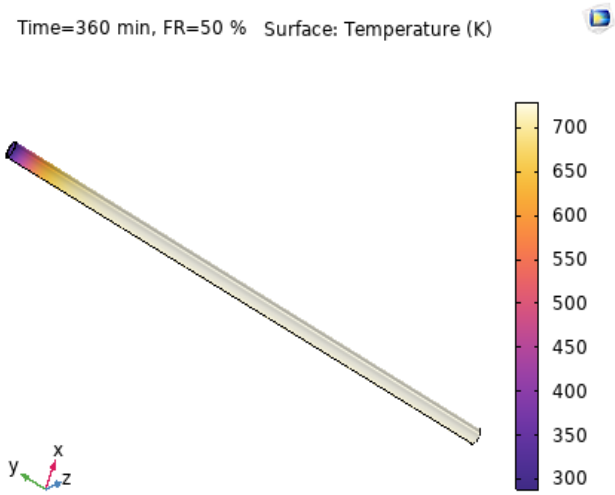
Time=360 min, FR=50 % Surface: Temperature (K)
700
650
600
550
500
450
400
350
300
x
y
z

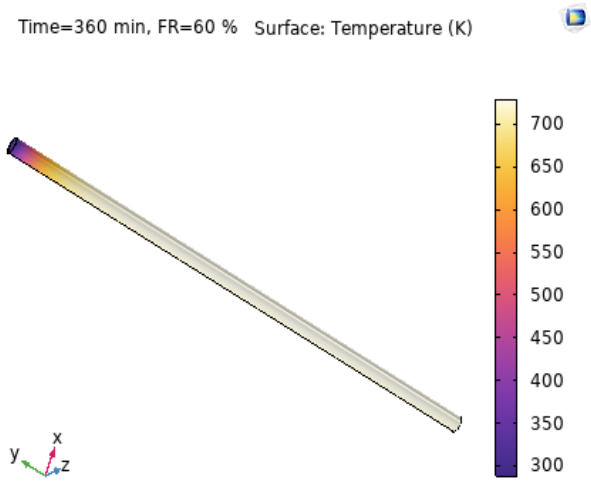
Time=360 min, FR=60 % Surface: Temperature (K)
700
650
600
550
500
450
400
350
300
x
y
z

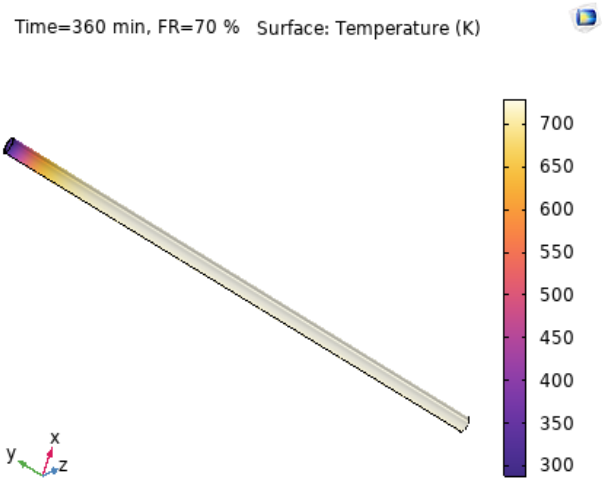
Time=360 min, FR=70 % Surface: Temperature (K)
700
650
600
550
500
450
400
350
300
x
y
z

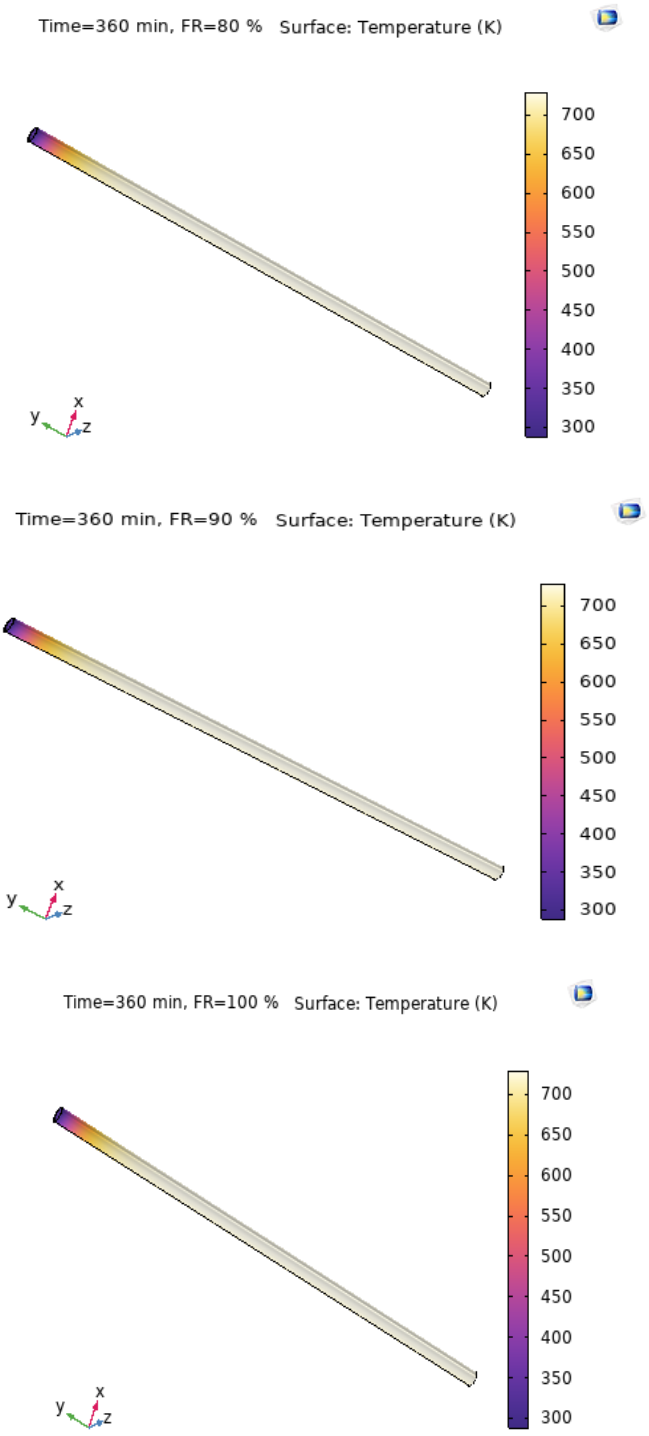

Figs. 4: Thermal distribution at different fill ratios, when T = 360min

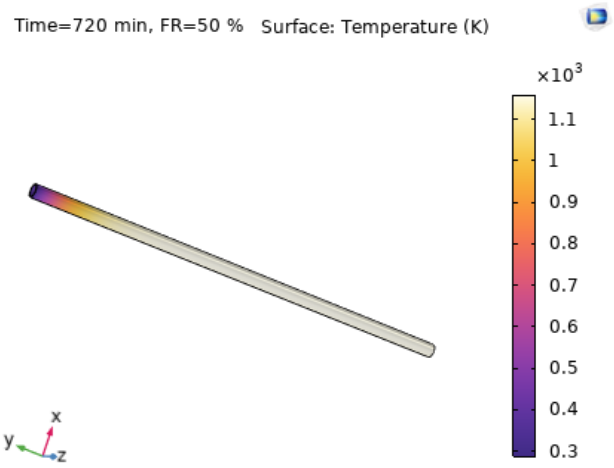
Time=720 min, FR=50 % Surface: Temperature (K)
×10^3
1.1
1
0.9
0.8
0.7
0.6
0.5
0.4
0.3
x
y
z

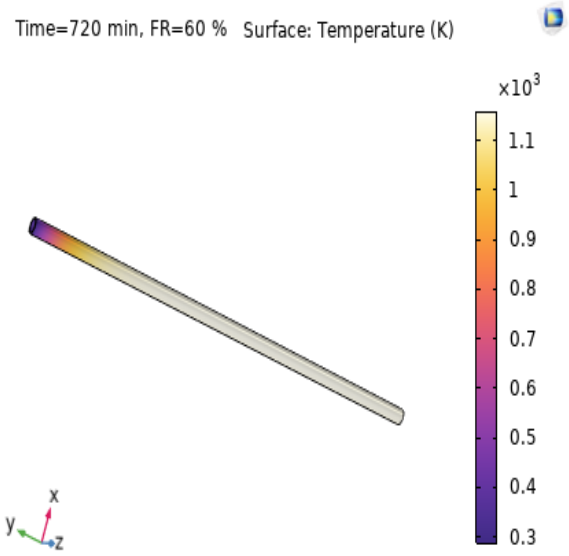
Time=720 min, FR=60 % Surface: Temperature (K)
×10^3
1.1
1
0.9
0.8
0.7
0.6
0.5
0.4
0.3
x
y
z

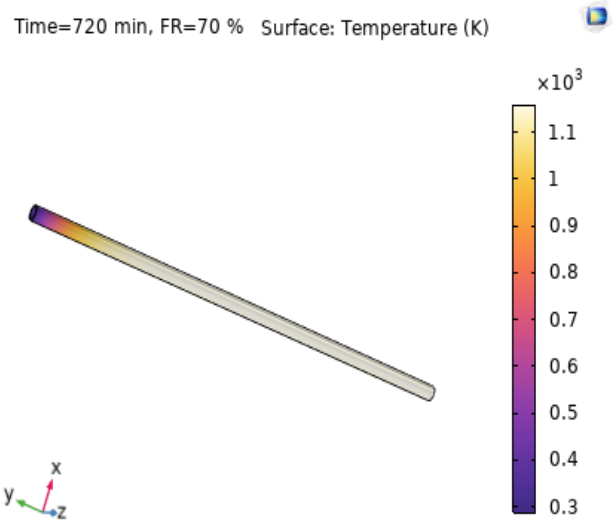
Time=720 min, FR=70 % Surface: Temperature (K)
×10^3
1.1
1
0.9
0.8
0.7
0.6
0.5
0.4
0.3
x
y
z

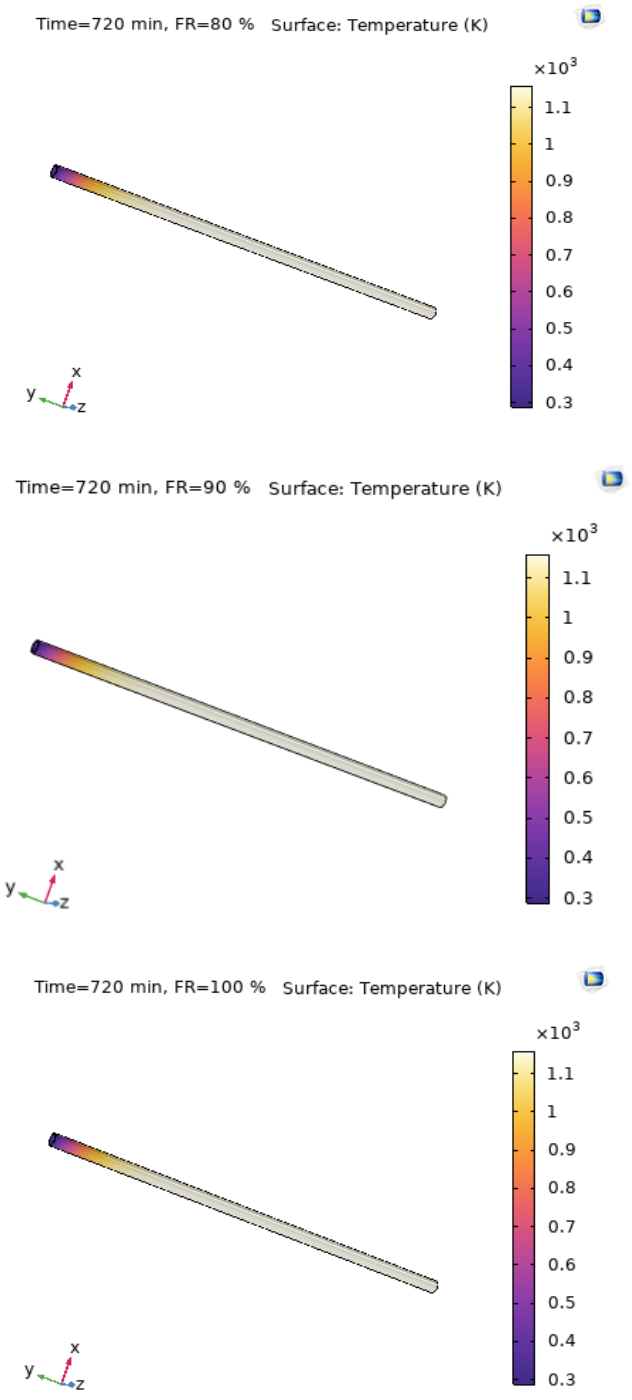

Figs. 5: Thermal distribution at different fill ratios, when T = 720min

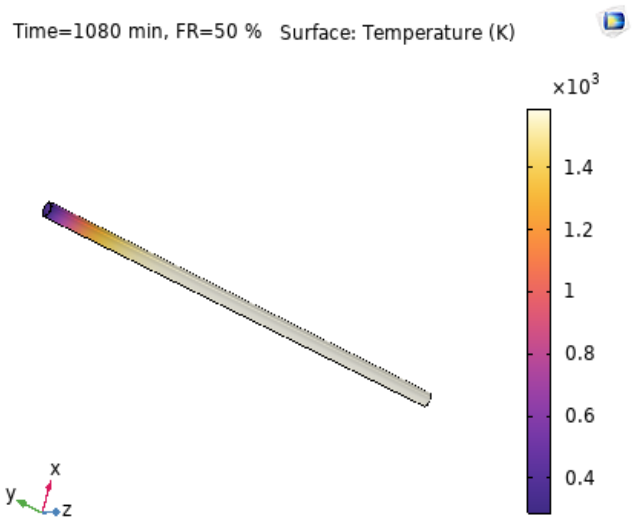
Time=1080 min, FR=50 % Surface: Temperature (K)
×10^3
1.4
1.2
1
0.8
0.6
0.4
x
y
z

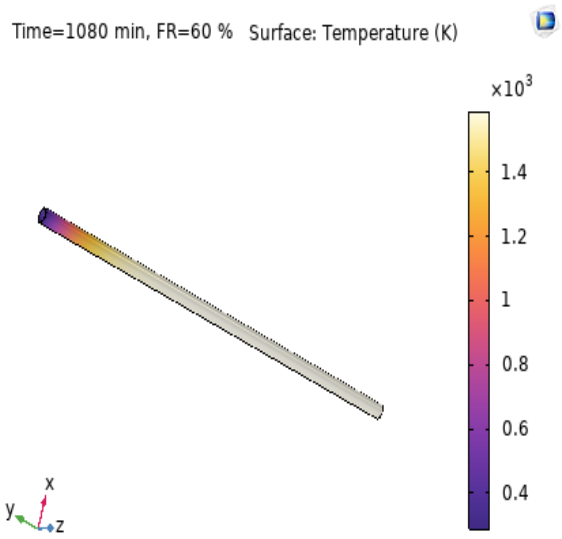
Time=1080 min, FR=60 % Surface: Temperature (K)
×10^3
1.4
1.2
1
0.8
0.6
0.4
x
y
z

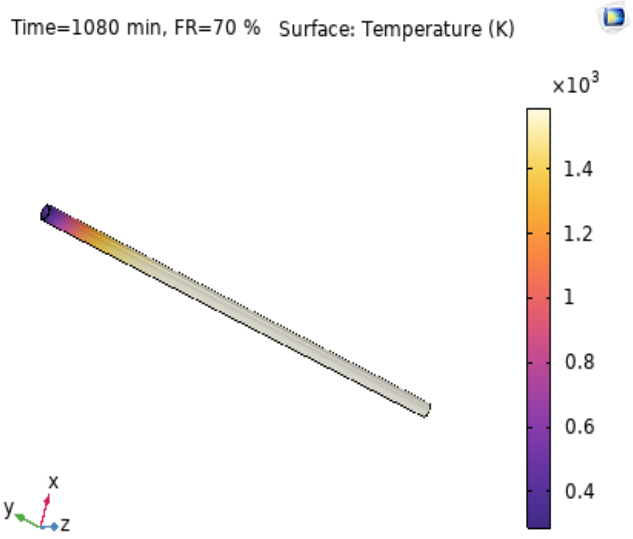
Time=1080 min, FR=70 % Surface: Temperature (K)
×10^3
1.4
1.2
1
0.8
0.6
0.4
x
y
z

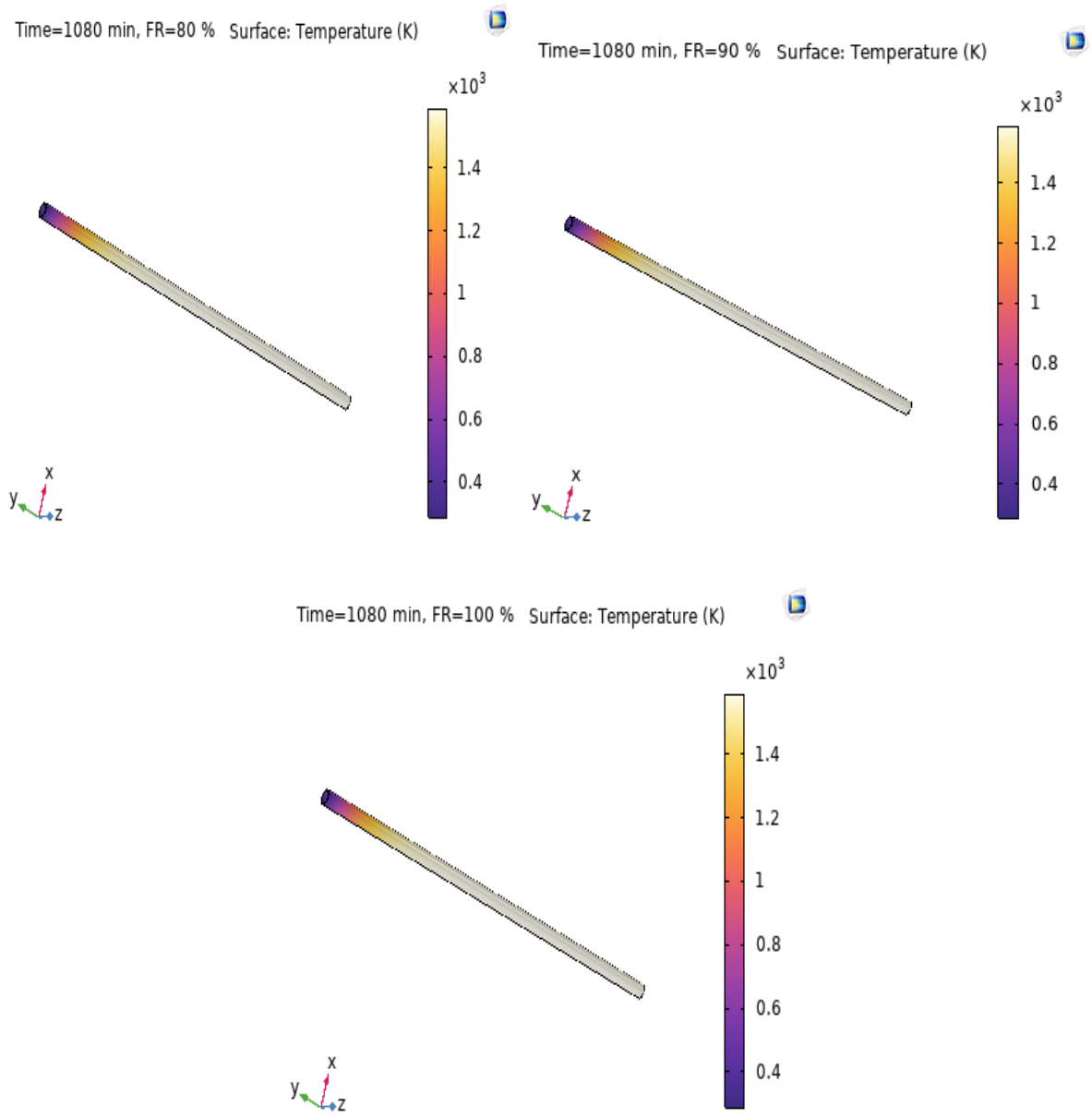

Figs. 6: Thermal distribution at different fill ratios, when T = 1080min

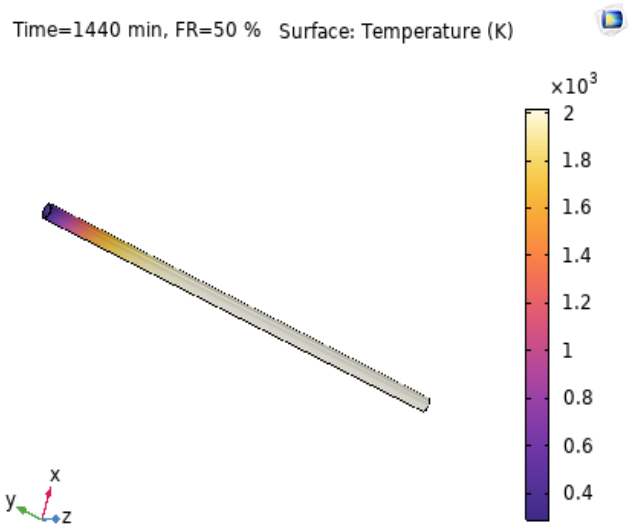
Time=1440 min, FR=50 % Surface: Temperature (K)
×10^3
2
1.8
1.6
1.4
1.2
1
0.8
0.6
0.4
x
y
z

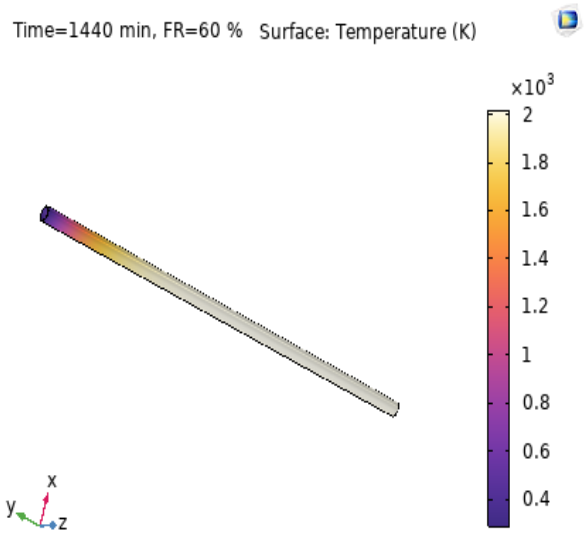
Time=1440 min, FR=60 % Surface: Temperature (K)
×10^3
2
1.8
1.6
1.4
1.2
1
0.8
0.6
0.4
x
y
z

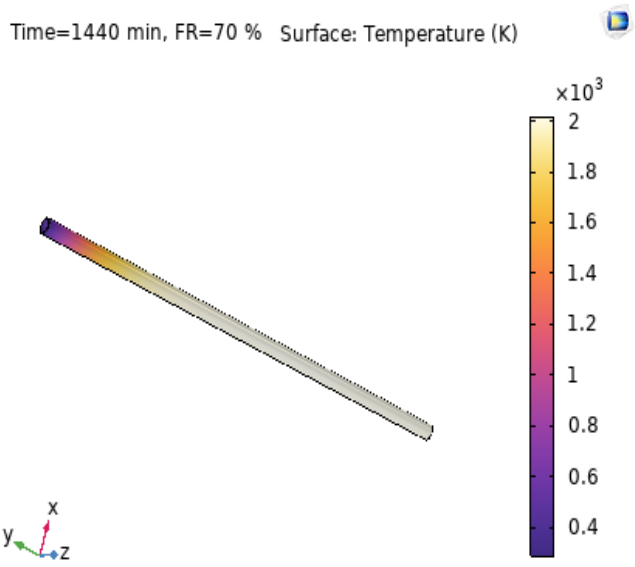
Time=1440 min, FR=70 % Surface: Temperature (K)
×10^3
2
1.8
1.6
1.4
1.2
1
0.8
0.6
0.4
x
y
z

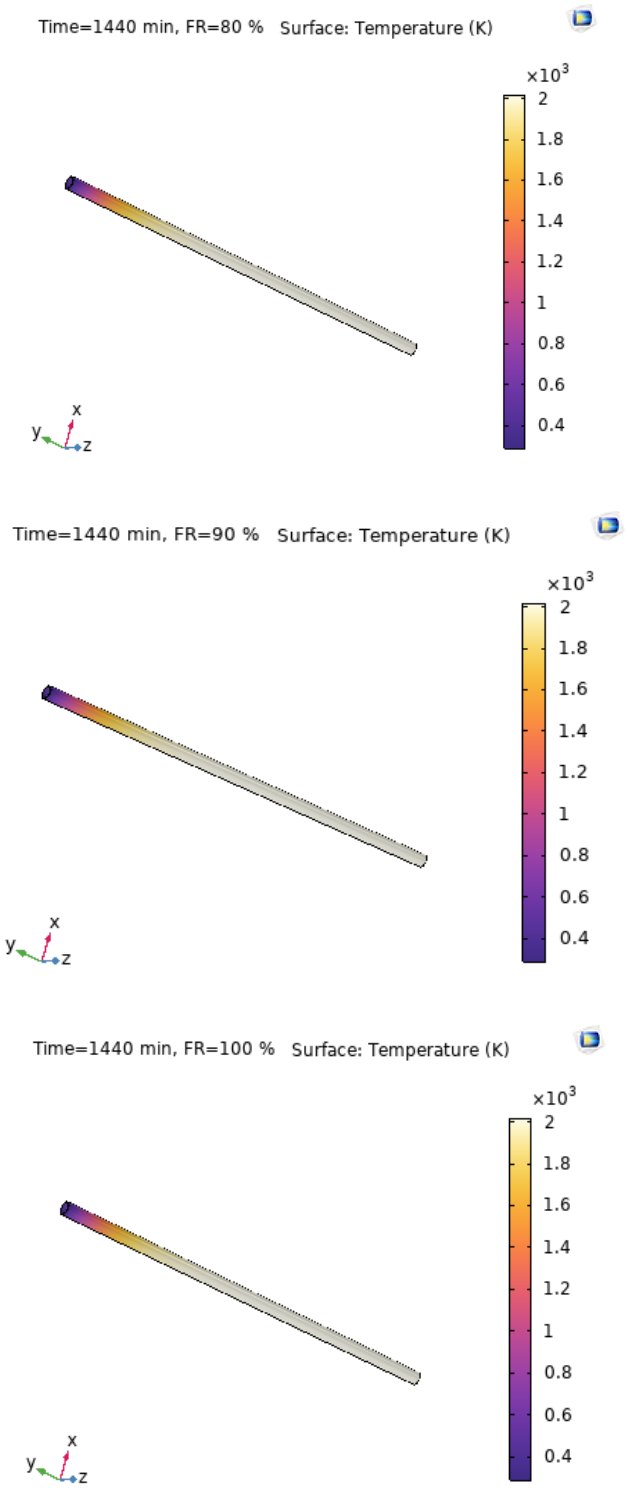

Figs. 7: Thermal distribution at different fill ratios, when T = 1440 min

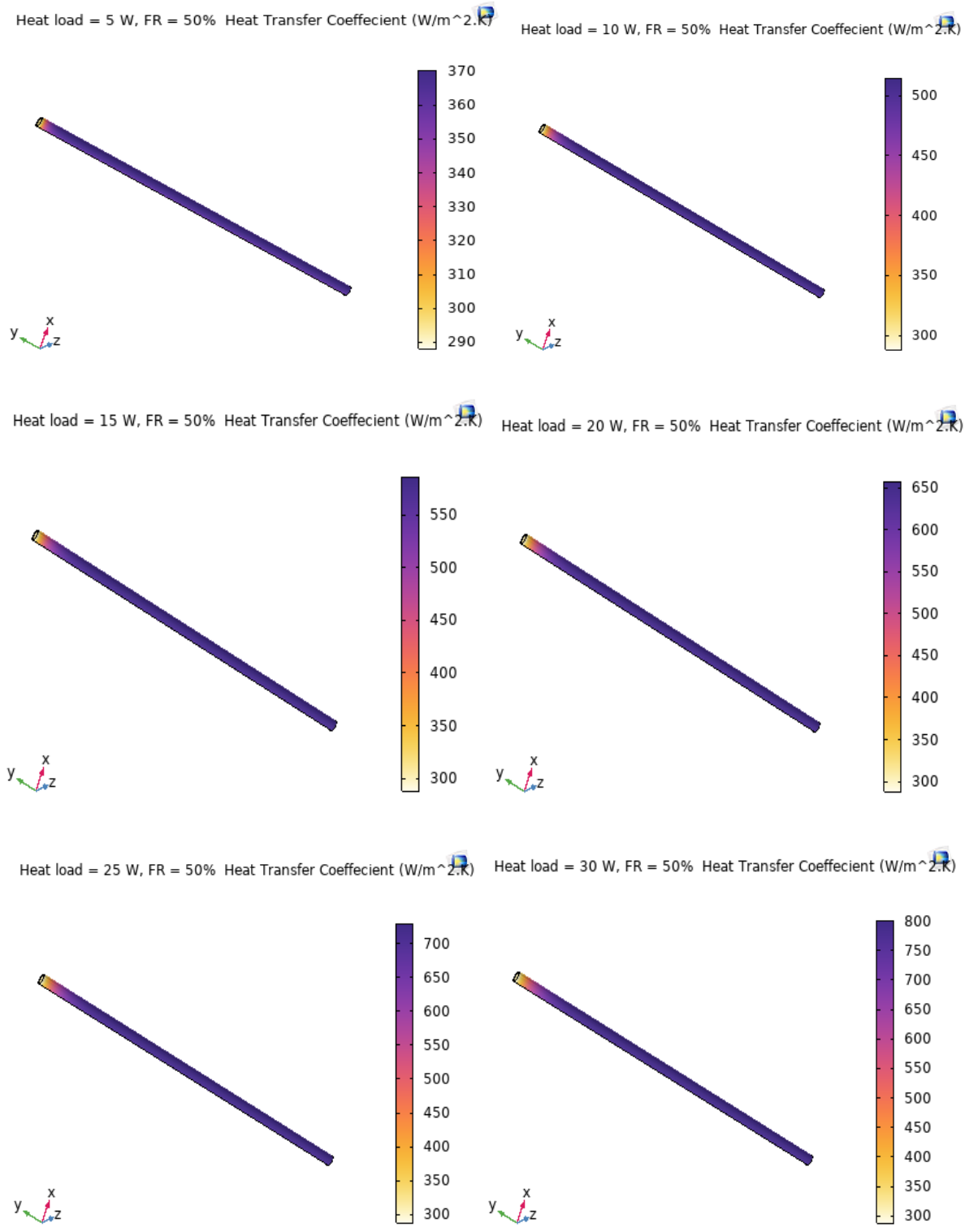

Figs. 8: Heat-transfer coefficient and input heat load at 50% filling ratio (FR)

5. Conclusion

Numerical models were employed to investigate heat transferred enhancement and performance of aqueous suspension in 0.2% volume concentration of Graphene-Oxide and water nanoparticles with varying fill charge ratios in a pipe channel at different temperatures. These insights can help optimize the design and operation of industrial processes involving fluid heat transfer, leading to increased productivity, reduce energy

consumption, and lower costs. The study revealed that heat transferred in pipe flow was enhanced with nanoparticle suspension, because the addition of GO nanoparticles to the working fluid significantly increased the performance of the heat pipe. However, it was discovered that heat transferred coefficient of heat pipe increased with increasing heating power and volumetric concentration of Nano-fluids, with pronounced effect on working fluid and filling ratio (FR). However, convective heat increased at high concentration of GO Nano-particles within base fluid and GO/water Nano-fluid revealed low thermal resistance. However, heat transferred coefficient of heat in pipe increases with increasing input power of 50% fill ratio at higher heat loads because of increase in rate of vaporization in working fluid.

Nomenclatures

Symbol	Identity	Unit
h	Coefficient of Heat Transferred	J/K
k	Thermal Conductivity	
Nu	Nusselt Number	
GO	Graphene-oxide	
m	mass	kg
p	pressure	N/m^2
q	rate of Heat Transferred	Joules (J)
r	radius of elastic pipe	m
Re	Reynolds Number	
T	Temperature	^oC
Ur	Velocity along radial direction	m/s
$U_\emptyset$	Velocity along azimuthal direction	m/s
U_x	Velocity along Axial direction	m/s
ρ	Density	kg/m^3
μ	Dynamic Viscosity	Pa.s
C_p	Specific Heat Capacity	J/kgK

References

[1] [1] J. L. Streator and D. B. Bogy, “Accounting for transducer dynamics in the measurement of friction,” *J. Tribol.*, vol. 114, no. 1, pp. 86–94, 1992, doi: 10.1115/1.2920873.

[2] [2] O. A. Adeaga, “Towards Numerical Investigation of Velocity Variation on Thin Ellipsoidal Aerofoil (NACA 3520) Using Surface Vorticity Method,” *2023 Int. Conf. Sci. Eng. Bus. Sustain. Dev. Goals*, vol. 1, no. Naca 3520, pp. 1–8, doi: 10.1109/SEB-SDG57117.2023.10124382.

[3] [3] M. Bang, S. Kim, S. Choi, H. S. Sohn, and H. H. Cho, “Impingement/effusion cooling with a hollow cylinder structure for additive manufacturing,” *Int. J. Heat Mass Transf.*, vol. 155, p. 119786, 2020, doi: 10.1016/j.ijheatmasstransfer.2020.119786.

[4] [4] S. Torii, “Enhancement of heat transfer performance in pipe flow using graphene-oxide-Nan0-fluid and its application,” *Mater. Today Proc.*, vol. 35, pp. 506–511, 2019, doi: 10.1016/j.matpr.2020.04.078.

[5] [5] W. W. Zhang, W. L. Cheng, S. D. Shao, L. J. Jiang, and D. L. Hong, “Integrated thermal control and system assessment in plug-chip spray cooling enclosure,” *Appl. Therm. Eng.*, vol. 108, pp. 104–114, 2016, doi: 10.1016/j.applthermaleng.2016.07.097.

[6] [6] T. J. Moore and M. R. Jones, “Solving nonlinear heat transfer problems using variation of parameters,” *Int. J. Therm. Sci.*, vol. 93, pp. 29–35, 2015, doi: 10.1016/j.ijthermalsci.2015.02.002.

[7] [7] T. Mukhtar, W. Jamshed, A. Aziz, and W. Al-Kouz, “Computational investigation of heat transfer in a flow subjected to magnetohydrodynamic of Maxwell Nan0-fluid over a stretched flat sheet with thermal radiation,” *Numer. Methods Partial Differ. Equ.*, no. September, pp. 1–21, 2020, doi: 10.1002/num.22643.

[8] [8] M. Cavazzuti, “Viscous heating effects on heat transfer characteristics of laminar compressible channel flow,” *Int. J. Heat Mass Transf.*, vol. 153, p. 119608, 2020, doi: 10.1016/j.ijheatmasstransfer.2020.119608.

[9] [9] Adeaga, O.A. Alabi, O.O. Akintola, S.A, “Experimental

Investigation Of The Potential Of Liquified," Vol. 17, no. 1, pp. 1–7, 2023.

[10] [10] M. A. Redo, K. Ohno, N. Giannetti, S. Yamaguchi, and K. Saito, "Seasonal performance evaluation of CO2 open refrigerated display cabinets," *Appl. Therm. Eng.*, vol. 163, no. September, p. 114354, 2019, doi: 10.1016/j.applthermaleng.2019.114354.

[11] [11] V. N. Constantinescu, "Thermal Effects in Incompressible Flow," pp. 203–235, 1995, doi: 10.1007/978-1-4612-4244-4_7.

[12] [12] I. A. Badruddin, "Investigation of heat transfer in irregular porous cavity subjected to various boundary conditions," *Int. J. Numer. Methods Heat Fluid Flow*, vol. 29, no. 1, pp. 418–447, 2019, doi: 10.1108/HFF-04-2018-0132.

[13] [13] J. Fang, N. Tu, J. F. Torres, J. Wei, and J. D. Pye, "Numerical investigation of the natural convective heat loss of a solar central cavity receiver with air curtain," *Appl. Therm. Eng.*, vol. 152, no. March 2018, pp. 147–159, 2019, doi: 10.1016/j.applthermaleng.2019.02.087.

[14] [14] H. S. Zhen, C. W. Leung, and C. S. Cheung, "Heat transfer from a turbulent swirling inverse diffusion flame to a flat surface," *Int. J. Heat Mass Transf.*, vol. 52, no. 11–12, pp. 2740–2748, 2009, doi: 10.1016/j.ijheatmasstransfer.2008.12.010.

[15] [15] S. E. Ibitoye, I. K. Adegun, P. O. Omoniyi, T. S. Ogedengbe, and O. O. Alabi, "Numerical investigation of thermo-physical properties of non-newtonian fliud in a modelled intestine," *J. Bioresour. Bioprod.*, vol. 5, no. 3, pp. 211–221, Aug. 2020, doi: 10.1016/j.jobab.2020.07.007.

[16] [16] K. Hu, J. Zhu, W. Zhang, K. Liu, and X. Lu, "Effects of evaporator superheat on system operation stability of an organic Rankine cycle," *Appl. Therm. Eng.*, vol. 111, pp. 793–801, 2017, doi: 10.1016/j.applthermaleng.2016.09.177.

[17] [17] S. E. Ibitoye, I. K. Adegun, O. A. Olayemi, P. O. Omoniyi, and O. O. Alabi, "Experimental and numerical investigation of flow behaviors of some selected food supplements in modeled intestine," *Sci. Iran.*, vol. 30, no. 1, pp. 39–51, Feb. 2022, doi: 10.24200/sci.2022.60130.6613.

[18] [18] P. Karimi Pour-Fard, E. Afshari, M. Ziaei-Rad, and S. Taghian-Dehaghani, "A numerical study on heat transfer enhancement and design of a heat exchanger with porous media in continuous hydrothermal flow synthesis system," *Chinese J. Chem. Eng.*, vol. 25, no. 10, pp. 1352–1359, 2017, doi: 10.1016/j.cjche.2017.01.015.

[19] [19] D. Tripathi, J. Prakash, M. Gnaneswara Reddy, and R. Kumar, "Numerical study of electroosmosis-induced alterations in peristaltic pumping of couple stress hybrid Nano-fluids through microchannel," *Indian J. Phys.*, vol. 95, no. 11, pp. 2411–2421, 2021, doi: 10.1007/s12648-020-01906-0.

[20] [20] S. Zhang, X. Xu, C. Liu, Y. Zhang, and C. Dang, "The buoyancy force and flow acceleration effects of supercritical CO2 on the turbulent heat transfer characteristics in heated vertical helically coiled tube," *Int. J. Heat Mass Transf.*, vol. 125, pp. 274–289, 2018, doi: 10.1016/j.ijheatmasstransfer.2018.04.033.

[21] [21] A. Zargoushi, F. Talebi, and S. H. Hosseini, "CFD modeling of industrial cold box with plate-fin heat exchanger: Focusing on phase change phenomenon," *Int. J. Heat Mass Transf.*, vol. 147, no. xxxx, p. 118936, 2020, doi: 10.1016/j.ijheatmasstransfer.2019.118936.

[22] [22] E. Pescini, F. Marra, M. G. De Giorgi, L. Francioso, and A. Ficarella, "Investigation of the boundary layer characteristics for assessing the DBD plasma actuator control of the separated flow at low Reynolds numbers," *Exp. Therm. Fluid Sci.*, vol. 81, pp. 482–498, 2017, doi: 10.1016/j.expthermflusci.2016.09.005.

[23] [23] S. Masood, M. Farooq, S. Ahmad, A. Anjum, and N. A. Mir, "Investigation of viscous dissipation in the Nan0-fluid flow with a Forchheimer porous medium: Modern transportation of heat and mass," *Eur. Phys. J. Plus*, vol. 134, no. 4, 2019, doi: 10.1140/epjp/i2019-12519-0.

[24] [24] I. K. Adegun, S. E. Ibitoye, and A.

Bala, "Effect of selected geometric parameters on natural convection in concentric square annulus," *Aust. J. Mech. Eng.*, vol. 20, no. 4, pp. 1142–1153, 2022, doi: 10.1080/14484846.2020.1784559.

[25] [25] S. A. M. Mehryan, M. Ghalambaz, A. J. Chamkha, and M. Izadi, "Numerical study on natural convection of Ag–MgO hybrid/water Nan0-fluid inside a porous enclosure: A local thermal non-equilibrium model," *Powder Technol.*, vol. 367, pp. 443–455, 2020, doi: 10.1016/j.powtec.2020.04.005.

[26] [26] O. A. Adeaga, A. A. Dare. "Cellular Vortex Element Modeling Of Multiphase Fluid Flow in Fractured Homogenous 3-D Oil Reservoir." *American Journal of Engineering Research (AJER),* vol. 6, no. 9, 2017, pp. 288–300.

[27] [27] O. A. Adeaga, A. A. Dare. "Potentials of Cellular Vortex Element Modeling of Fluid Flow in Confined 2D Aquifer'' *Journal of Energy and Power Engineering* 10 (2016) 137-149 doi:10.17265/1934-8975/2016.03.001